Characterization of the atmosphere with the Sky Monitor

4RD-20-NO.rev00-2026-11-13

Introduction

Miratlas enables optical communications between Earth and space by addressing the issue of light propagation in the atmosphere.

Free Space Optical Communications (FSOC) use light to carry data instead of traditional radio frequencies (RF) communications. FSOC offer many advantages over RF: faster transmission of data, more robust to interception, compatible with quantum key distribution, lower interference, lower power consumption, lighter and more compact instruments and cost-effectiveness.

Nevertheless, light signals are much more sensitive to attenuation and distortion than other electromagnetic waves. A light signal is stopped by **clouds**, attenuated by **aerosols** and distorted by **turbulences.** Local weather parameters (especially humidity and surface wind) cause secondary impact. These physical obstacles are unavoidable but can be mitigated with dedicated technologies and informed decisions.

Miratlas offers solutions to monitor atmosphere turbulence, cloud-cover and aerosols, providing useful information for the selection of optimal Optical Ground Stations (OGS) sites, their design, and supporting live operations of laser communication networks. Turbulence can be mitigated with different technics (adaptive optics for example), whereas only site diversity can overcome cloud-cover.

The Sky Monitor characterizes the atmosphere autonomously, by day and night. Its compact design is compatible with outdoor operation and easy to deploy on any location. It requires no photometric calibration, nor large optics, nor a dome. Its standard design makes the comparison easier from one site to another.

Key atmospheric parameters

The CCSDS (Consultative Committee for Space Data Systems) Optical Communication workgroup has listed key atmospheric parameters which affect space-to-ground FSOC [1]. The following section presents the parameters measured by Miratlas' instruments, following the recommendations of the CCSDS: cloud cover, turbulence, aerosol and weather.

Cloud cover

Depending on their type, clouds attenuate or even completely block the optical signal. While cirrus clouds (high altitude and thin clouds) cut down the power of the signal of a few dB, most clouds attenuate the signal of hundreds of dB, blocking communication.

The parameters characterizing the cloud cover are the **total cloud cover** (percentage of the sky on a given location that is block by clouds) and the **transparency of the sky**.

Clouds are monitored with allsky cameras, they can be detected in the visible spectrum, but infrared imaging offers images with sharper cloud segmentation.

Turbulence

Turbulence is due to inhomogeneities of temperature, pressure and humidity in the atmosphere, inducing variations of the refractive index which affect the propagation of light. The refractive index structure parameter C_n^2 primarily describes the strength of turbulence, this quantity is derived into other integrated parameters: Fried parameter r_0, *seeing*, isoplanatic angle θ_0, scintillation index σ_I^2 and coherence time τ_0.

Turbulence parameters depend on the wavelength of the optical signal, and the elevation at which they are measured. For easing comparisons, all parameters measured by Miratlas' instruments are given at a wavelength λ of 550 nm and corrected to zenith, the zenith angle ζ equals 0.

Refractive index structure parameter C_n^2

The **refractive index structure parameter**, denoted $\boldsymbol{C_n^2}$, is the distribution of the turbulence strength along the altitude from ground. It is given in $m^{-2/3}$, usually ranging from 10^{-12} to 10^{-18} $m^{-2/3}$.

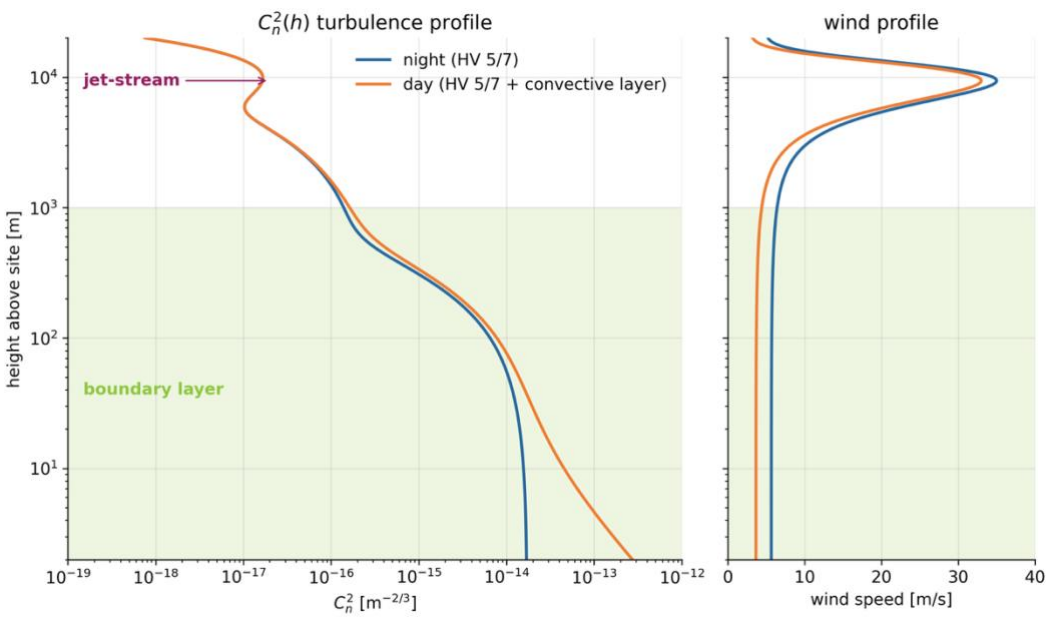


Figure 1 Illustration of standard C_n^2 profile (from Hufnagel-Valley 5/7 model) and wind profile (Bufton model). Turbulence varies from day to night, especially in the boundary layer, and along altitude from ground.

Figure 1 illustrates standard turbulence and wind profiles, respectively based on Hufnagel-Valley and Bufton models. Turbulence is stronger close to the ground, and a bump appears on the profiles around 10 km due to jet-stream winds. The boundary layer height is set to 1 km for the illustration only, highest C_n^2 values are lying under this height.

Fried parameter r_0 and seeing

The **Fried parameter**, denoted $\boldsymbol{r_0}$, is the characteristic spatial dimension of turbulence. It represents the diameter over which the wavefront remains undistorted, more precisely the rms wavefront aberration is 1 rad. The Fried parameter is a key measure of the strength of the turbulence integrated over the whole airmass from ground level to the top of the atmosphere. A large r_0 value indicates low atmospheric turbulence.

It is provided in cm, ranging from about $1\ cm$ in strong turbulence, up to more than $20\ cm$ under favorable conditions. Low altitude turbulence has a prominent impact on the Fried parameter value.

From a user point of view, the Fried parameter indicates how complex must the turbulence mitigation be. The ratio $D\ /\ r_0$, with D the diameter of the telescope, determines the number of Zernike modes to correct.

The analytical definition of Fried parameter is:

$$r_0 = \left[0.423 \times (2\pi/\lambda)^2 \times \cos^{-1}\zeta \times \int C_n^2(h)dh\right]^{-3/5} \quad [1]$$

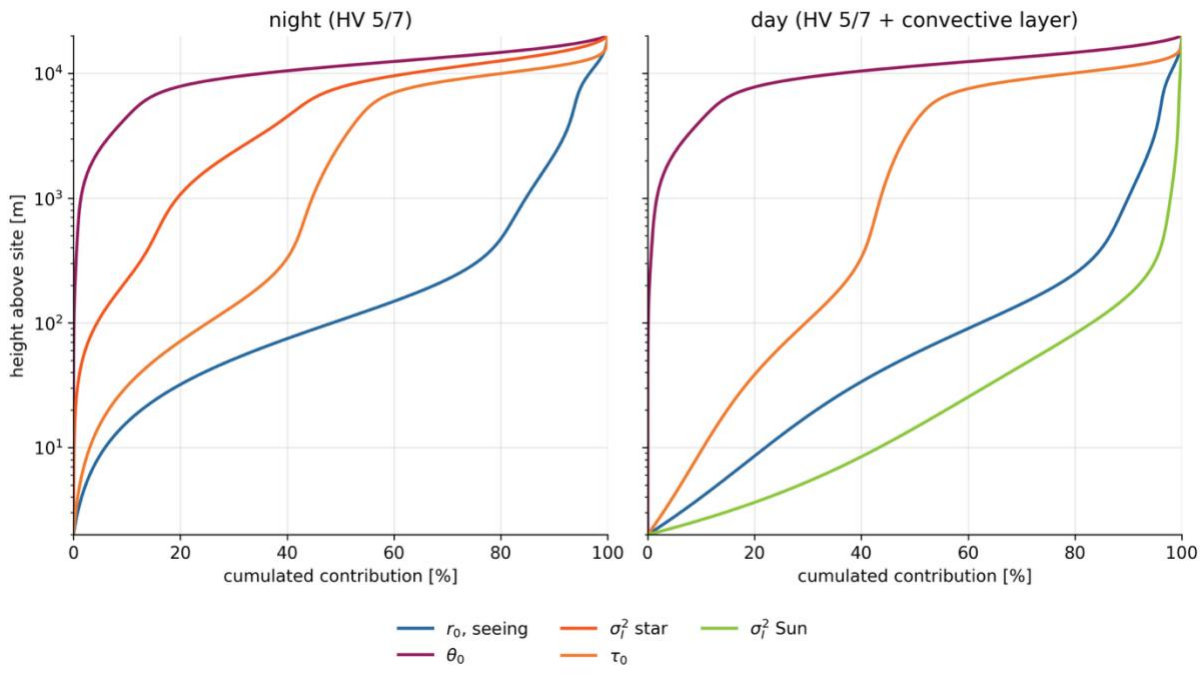


Figure 2 Cumulated contribution of turbulence at different altitude to the values of integrated parameters, from a modeled Hufnagel-Valley turbulence profile.

Figure 2 represents the cumulated contribution of turbulence at a given altitude to the integrated parameters values. The lines are calculated from the modeled Hufnagel-Valley profiles introduced in Figure 1. In this configuration, turbulence under 1 km contributes to more than 80% of Fried parameter r_0 and seeing by day and night.

Figure 3 shows examples of turbulent phase screens distorting the wavefront of light signal going through the atmosphere. The dimension of the Fried parameter is represented at the bottom left of each image, it is smaller by day because turbulence is stronger.

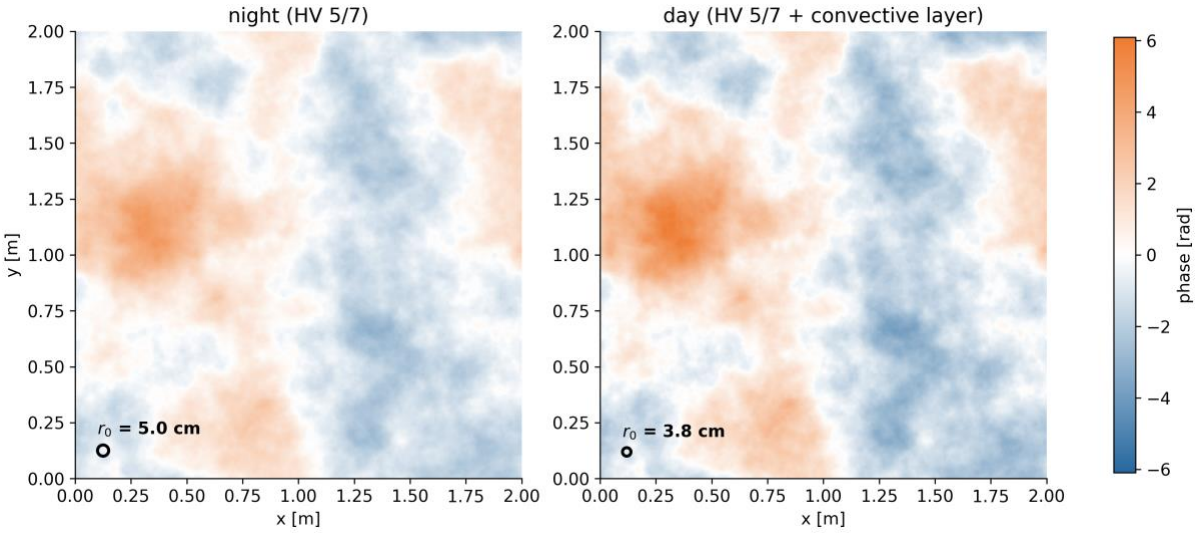


Figure 3 Examples of turbulent phase screen generated from modeled Hufnagel-Valley turbulence profiles. The Fried parameter is represented at the bottom left of each phase screen.

The ***seeing*** ϵ is inversely proportional to Fried parameter. Given in $arsec$, this parameter is more commonly used by astronomers.

$$\epsilon = 0.98 \times \lambda / r_0 \qquad [2]$$

Isoplanatic angle θ_0

The **isoplanatic angle**, denoted $\boldsymbol{\theta_0}$, is the characteristic angular dimension of turbulence. It refers to the maximum angle over which the wavefront remains unperturbed over the entire distance between the transmitter and receiver.

It is provided in $arcsec$, ranging around a few arcseconds. High altitude turbulence has a prominent impact on the isoplanatic angle value as shown in Figure 2.

From a user point of view, the isoplanatic angle determines the penalty on the point-ahead angle. As satellites are moving quickly relatively to the ground station, turbulence endured by the downlink may differ from the one affecting the uplink.

The analytical definition of isoplanatic angle is:

$$\theta_0 = \left[2.905 \times (2\pi/\lambda)^2 \times \cos^{-8/3}\zeta \times \int C_n^2(h) h^{5/3} dh\right]^{-3/5} \qquad [3]$$

Scintillation

Scintillation represents the random variations in the intensity of the optical signal as it propagates through the atmosphere. These intensity fluctuations cause the signal to fade, flicker, or twinkle.

Various parameters characterize the scintillation, including **scintillation index** $\boldsymbol{\sigma_I^2}$ and the **rytov number** $\boldsymbol{\sigma_R^2}$. These parameters are dimensionless.

Coherence time τ_0

The **coherence time**, denoted $\boldsymbol{\tau_0}$, is the characteristic time of turbulence. It refers to the duration over which the received optical signal maintains a coherent phase relationship with the transmitted signal.

It is given in ms, its values are typically of a few miliseconds.

From a user point of view, the τ_0 value determines the maximum time response of the mitigation technology to compensate the distortion of the signal.

Coherence time depends on Fried parameter and **effective windspeed** $\bar{v}$, the latter is a scalar representative of the distribution of wind speed along the full atmosphere height.

$$\tau_0 = 0.314 \times r_0/\bar{v} \quad [4]$$

$$\bar{v} = \left[\frac{\int C_n^2(h) v^{5/3}(h) dh}{\int C_n^2(h) dh}\right]^{3/5} \quad [5]$$

Aerosols

Irradiance

The brightness of the sky adds noise while receiving optical signal from space, this noise interferes with signal reception. This sky brightness is due to both natural and artificial factors.

Water vapor

Water vapor in the atmosphere significantly attenuates light signal due to absorption. The **precipitable water column** (PWC), also denoted precipitable water vapor, characterizes the water vapor in a vertical column in the atmosphere. Specifically, it is the equivalent amount of liquid water produced if all the water vapor in the column were to condense and fall as precipitation.

It is provided in cm, which values ranging from 0 to about 20 centimeters.

Weather

Meteorological parameters measured at ground level such as **temperature**, **pressure**, **relative humidity**, **wind** and **rain**, are useful to correlate turbulence measurements with atmospheric conditions.

Overview of Miratlas Sky Monitor

C-DIMM

Acquired data: **nighttime Fried parameter $\boldsymbol{r_0}$**, ***seeing***, **isoplanatic angle $\boldsymbol{\theta_0}$** and **coherence time $\boldsymbol{\tau_0}$**

The C-DIMM is a Compact Differential Image Motion Monitor, based on the proven DIMM technic developed by astronomer for nighttime turbulence monitoring [2–5]. It uses two optical tubes of 49 mm of diameter, separated by 200 mm, with synchronized cameras pointing the same star. The relative motion of the images in longitudinal and transverse directions is proportional to the angle of

arrival of the wavefront of the light which has gone through the atmosphere. The position of the star on an image is determined by the position of its barycenter. The C-DIMM measures turbulence every minute by night, under clear sky.

The Fried parameter and the *seeing* are calculated from the variance of relative distance between the barycenter of the two images during a series of acquisitions, in longitudinal and transverse directions.

The isoplanatic angle is determined from the variance of the normalized intensity of the light collected on the images.

The coherence time depends on the Fried parameter and the effective wind speed. This latter parameter is measured from the temporal decorrelation of the images.

The C-DIMM is sensitive to the whole atmosphere height. It sees both low altitude and high-altitude turbulence. By default, it only points Polaris star in the Northern hemisphere, on a fixed setup. For other locations and measurements in different directions, the C-DIMM can be set on a motorized mount which tracks different stars every night.

Motion common to both images, such as system vibrations, wind-induced shake, and tracking or guiding errors, cancels out by construction. Only the atmospheric component remains, and its variance is directly related to the Fried parameter r_0. Single-aperture systems, which measure either the absolute image motion or the long-exposure full width at half maximum (FWHM), are by contrast contaminated by these mechanical disturbances. They therefore require a highly stable mount and rigorous guiding, and it is not always possible to separate the instrumental contribution from the atmospheric one. The C-DIMM is also considerably less sensitive to the outer scale L_0 of turbulence. Absolute tip/tilt, which carries most of the phase variance, is strongly attenuated by a finite outer scale, whereas the differential motion, measured at the scale of the baseline, remains close to the Kolmogorov regime in which r_0 is defined. The measurement is therefore more representative and more readily comparable from one site to another.

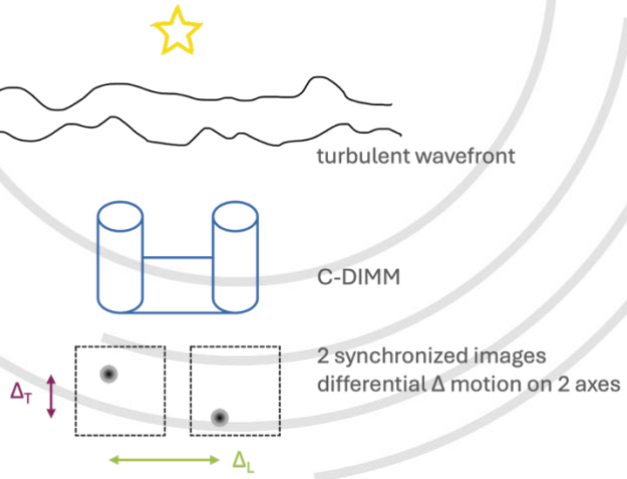


Figure 4 The C-DIMM infers Fried parameter from the differential motion of two images of the same star.

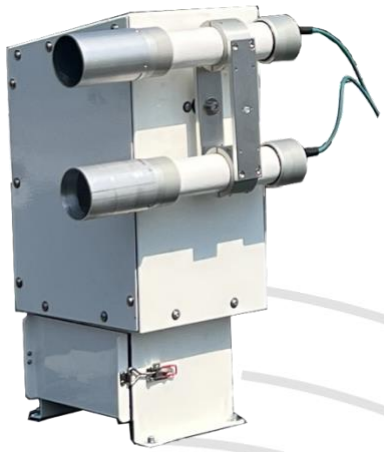


Figure 5 The C-DIMM can either be installed on a motorized mount to track different stars, or set in a fixed position, pointing Polaris star (in Northern hemisphere only).

DN-DIMM

Acquired data: **daytime and nighttime Fried parameter r_0, *seeing*, isoplanatic angle θ_0** and **coherence time τ_0**

Whereas the standard C-DIMM is only compatible with nighttime operations, the DN-DIMM (Day and Night DIMM) relies on the exact same principle but works by day and by night. The instrument measures turbulence every minute, continuously from day to night without any interruption at dawn or dusk and stands outdoor with no dome. It has a more elaborated design (larger apertures and optics, spectral filters, focusers…) and requires a motorized mount to point and track stars.

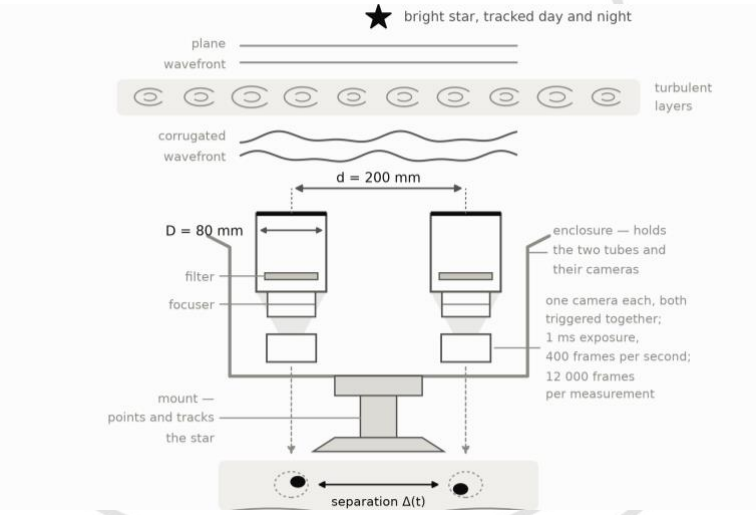


Figure 6 Using the same standard DIMM design, the DN-DIMM measures turbulence by day and by night.

SHABAR

Acquired data: **daytime turbulence profile C_n^2, Fried parameter r_0, *seeing*** and **isoplanatic angle θ_0**

The SHABAR (SHAdow BAnd Ranger) is a daytime turbulence profiler designed to measure the refractive index structure constant C_n^2 as a function of altitude within the boundary layer by using solar scintillation [6–9]. It measures a turbulence profile every minute by day, under clear sky.



Figure 7 The SHABAR has six photosensors installed on a motorized mount to track the Sun during daytime.

It presents an array of six photodiodes. The signal collected on each channel corresponds to the solar intensity fluctuations perturbated by atmospheric turbulence. Each sensor is sensitive to turbulence within a cone extending from the sensor to the solar disk. The correlation between the signal of two separated sensors depends on their respective distance. The closer the sensors, the higher the correlation, as their observation cones intersect over a larger volume. The altitude at which the cones intersect also varies with the separation distance. The determination of turbulence at different altitudes is based on the analysis of the covariances of the six channels.

The SHABAR is only sensitive up to approximately 1 kilometer from ground, where most of turbulence lies during daytime. It cannot see high altitude-turbulence.

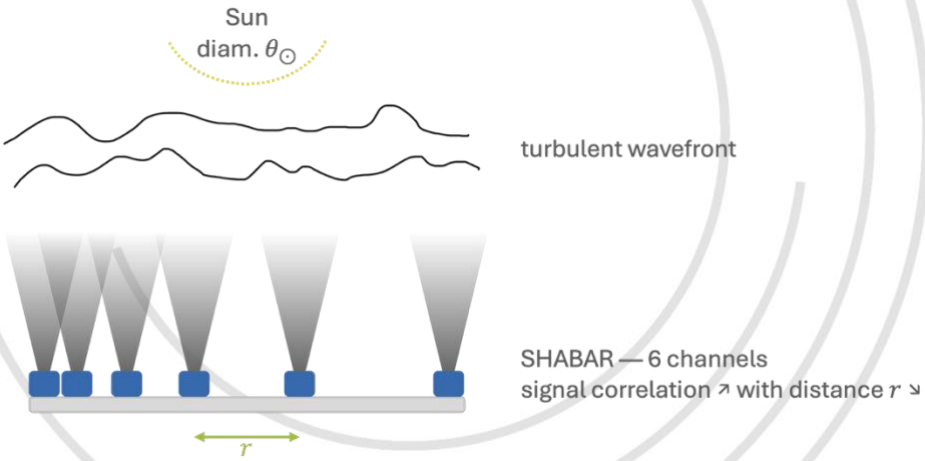


Figure 8 Each sensor is sensitive to turbulence within a cone extending from the sensor to the solar disk. The closer the sensors, the higher the correlation of their signals.

Main unit

The main unit of the Sky Monitor embeds various sensors and a computer for control, data collection and processing. The system and the results are accessible by the user remotely.

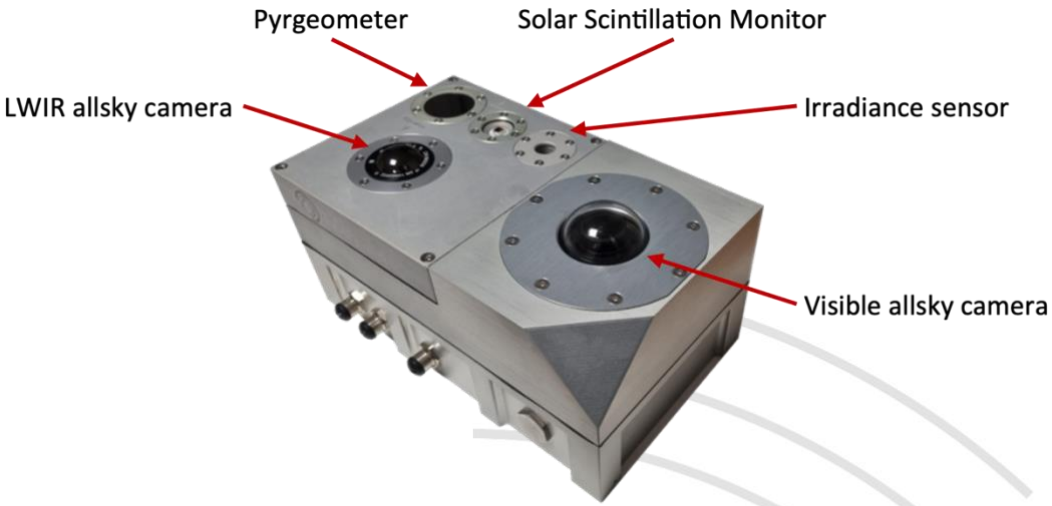


Figure 9 The main unit of the Sky Monitor embeds several sensors and a computer.

The following sections provide details on the onboarded sensors: Solar Scintillation Monitor, Allsky cameras, visible and LWIR, Irradiance sensor and Pyrgeometer

Solar Scintillation Monitor

Acquired data: **daytime *seeing*** and **Fried parameter r_0**.

The Solar Scintillation Monitor (SSM) is a daytime *seeing* monitor developed in the 1990's from the observation of a correlation between scintillation of solar intensity signal and image quality. [6,7,10,11]

The photosensor is embedded in the main unit of the Sky Monitor and estimates the number of turbulence cells included in the solar disk from the scintillation of light intensity and then calculates *seeing*. The Fried parameter r_0 is calculated from the *seeing* value every minute.

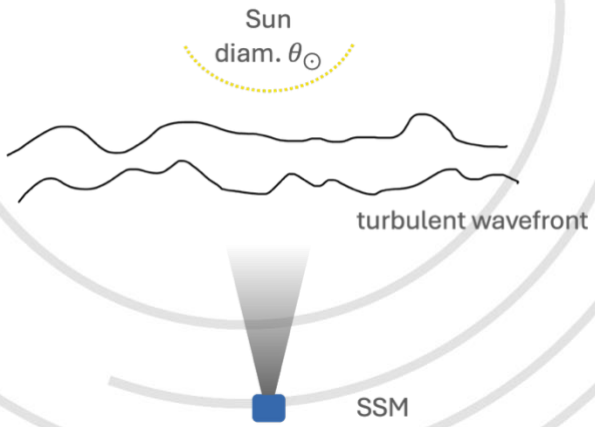


Figure 10 SSM infers seeing from the scintillation of the Sun, it probes only close to the ground.

This measurement is only sensitive to the lowest layers of the atmosphere, from ground level up to a few hundreds of meters. The Sun being an extended source (apparent diameter $\theta_\odot \approx 9.3\ mrad$), the intensity fluctuations produced by a layer at altitude h are averaged over a scale $h\theta_\odot$. At high altitude, the size of the patch over which the fluctuations are integrated is very large, the averaging cancels out the variations. Therefore, only the lower layers contribute significantly to the signal.

Allsky cameras, visible and LWIR

Acquired data:

- visible camera: monochrome visible **allsky images** and nighttime **transparency map**
- LWIR camera (option): **thermal allsky images**

A camera with a fisheye lens provides whole sky images in the visible spectrum every 5 minutes. The images have an effective size of 2064 x 20264 pixels with a monochrome dynamic of height bits (256 ADU levels). The optics does not deliver f-theta images, they are corrected during the post-processing. The camera has an automatic gain and exposure time ranging from a few microseconds during daytime, to 10 s at night.

Another camera with a fisheye lens provides whole sky images in the long wave infrared (LWIR) spectrum every 5 minutes, it delivers *f*-theta corrected images.

The daytime visible images are processed to identify clouds, determine a cloud mask and calculate a percentage of clear sky as presented in Figure 11. This approach is limited by the light halo formed around the Sun, and the difficulties to discriminate overcast from clear sky under some conditions. Thermal images are more reliable for cloud detection under any conditions. Clouds are warmer than sky background, a cloud mask is simply determined with a threshold applied on the temperature values.

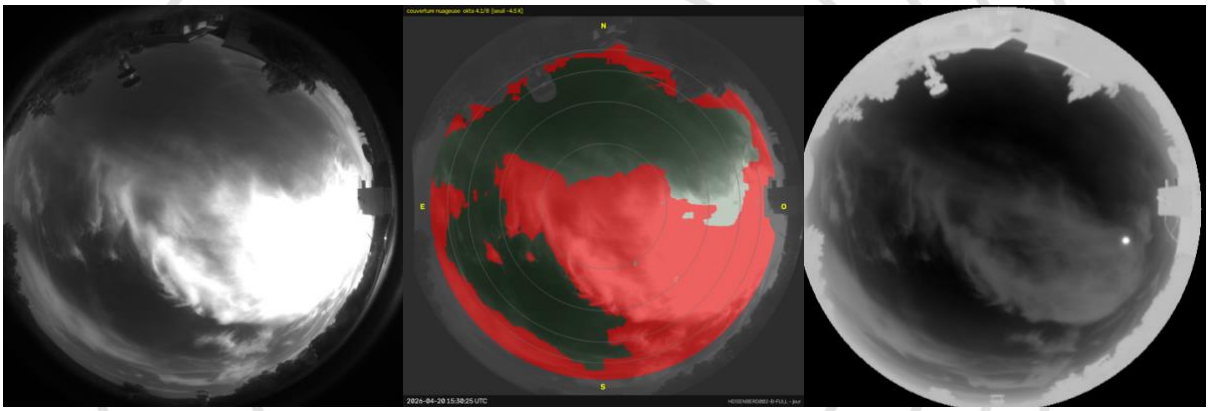


Figure 11 Visible (left) and thermal (right) allsky images in Observatoire de Haute Provence on April 20th, 2026 at 15:30. Clouds are easier to see on thermal images, the Sun appears as a disk and not a halo. The image in the middle is the visible allsky image with an overlay of cloud segmentation.

By night, the allsky visible camera can detect stars with magnitude lower than 6.75, which is more than 2000 stars on a single image. An astrometric resolution identifies the stars and is used to calculate a nighttime transparency map, as shown on Figure 12. Clouds can sometimes not be clearly seen on the visible images by night, but their presence is inferred from the transparency measurement. If a star is not seen at its position, then a cloud is hiding this given star. The Moon can also generate a halo on the images.

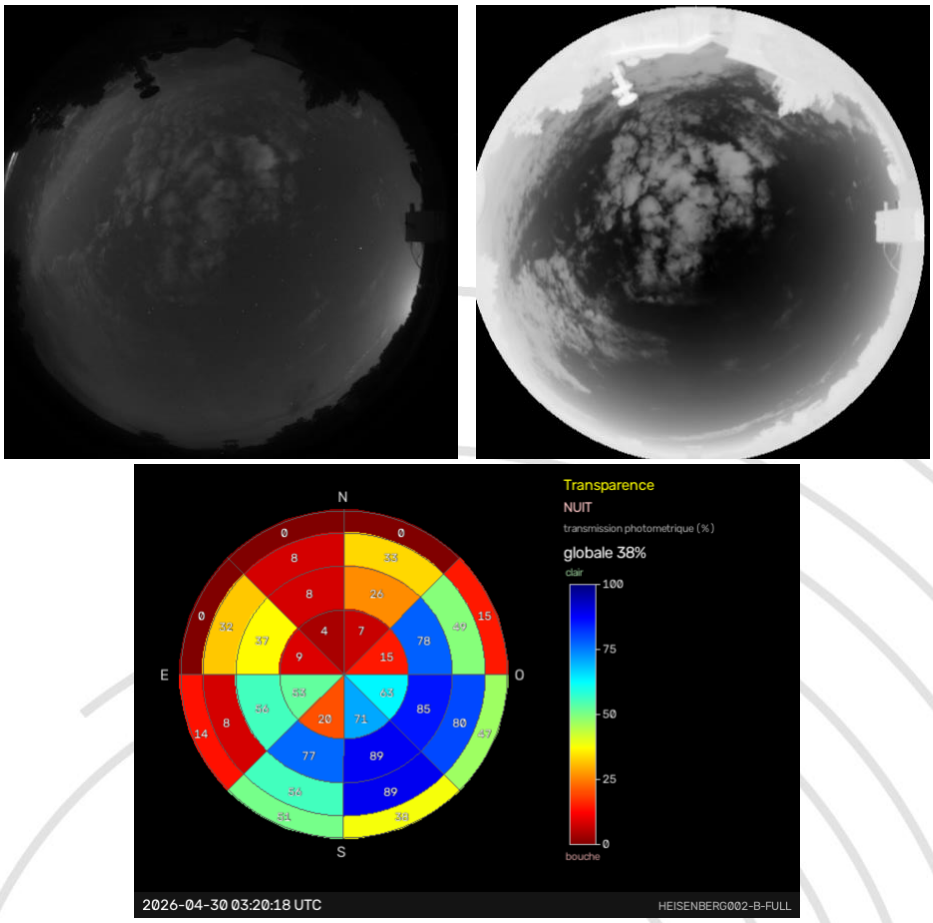


Figure 12 Visible (top left) and thermal (top right) allsky images by night. Transparency maps (bottom) is calculated from the analysis of the visible allsky image and the identification of stars.

As presented in Figure 12, the sky is divided into 32 regions (4 rings and 8 quarters), five parameters are calculated for all cells: photometric transmission, percentage of clear sky (same as during daytime), availability for a laser link, magnitude depth and attenuation at 1550 nm. A classification of laser link opportunities is inferred from all this analysis.

The cloud cover monitoring works from day to night, without interruption.

Irradiance sensor

Acquired data: **irradiance**

A large dynamic photodiode gives the sky irradiance in $mag/arcsec^2$. It has a 40° field of view to reduce the influence of local straylight. The sensor gives a rough estimation of light pollution and backscattered light in urban environment, one measurement per minute.

Pyrgeometer

Acquired data: **sky temperature** at zenith, **back scattered thermal radiation** and **precipitable water column**

Two long wave infrared (LWIR) radiometric thermopiles measure temperature of the sky, one facing zenith with a 10° field of view, the other facing the opposite direction of the equator at an elevation of 52°. These sensors deliver the temperature of the sky. They are useful to check if the zenith is clear or cloudy (background sky is colder than clouds and ambient air at ground level), and to calculate the back

scattered thermal radiation. Precipitable water column (PWC) is roughly estimated from the temperature of the sky. The measurements are made every minute.

Weather station

Acquired data: **temperature**, **pressure**, **relative humidity**, **wind** and **rain**

A calibrated weather station measures local weather parameters every minute. A heatshield protects pressure, temperature, and humidity sensors, while wind is measured with 2D ultrasonic anemometers and rain rate is measured with a piezoelectric sensor.



Figure 13 The weather station embeds several sensors.

Conclusion

The Sky Monitor measures the key atmospheric parameters for free-space optical communications: turbulence and clouds. It provides daytime turbulence profile C_n^2, daytime and nighttime *seeing*, Fried parameter r_0 and isoplanatic angle θ_0, and nighttime coherence time τ_0.

By night, the C-DIMM measures turbulence using the stars: *seeing*, Fried parameter r_0, isoplanatic angle θ_0, and coherence time τ_0. It is sensitive to the whole atmosphere height and is more robust than single aperture systems.

By day, the SSM and the SHABAR measure turbulence using the Sun: C_n^2 profile, *seeing* and Fried parameter r_0. They are only sensitive to the lower layers of the atmosphere (up to several hundreds of meters), where most of turbulence lies during daytime.

The DN-DIMM bridges the gap and measures turbulence integrated parameters continuously: *seeing*, Fried parameter r_0, isoplanatic angle θ_0, and coherence time τ_0. It is sensitive to the whole atmosphere height as well.

The monitoring of cloud-cover by day and by night uses allsky images in the visible and LWIR spectrums.

The overall system is easy to install, autonomous and accessible with a remote interface. Its compact design is weather-proof, it requires no calibration, nor large optics, nor a dome.

The measurements provided are useful for the selection of sites for optical ground stations, their design and their operation.

References

1. Consultative Committee for Space Data Systems (CCSDS), "Atmospheric Characterization and Forecasting for Optical Link Operations," (2022).
2. M. Sarazin and F. Roddier, "The ESO differential image motion monitor," Astron. Astrophys. **227**, 294–300 (1990).
3. M. Sarazin and A. Tokovinin, "The Statistics of Isoplanatic Angle and Adaptive Optics Time Constant derived from DIMM Data," in (2002), Vol. 58, p. 321.
4. A. Tokovinin, "From Differential Image Motion to Seeing," Publ. Astron. Soc. Pac. **114**, 1156 (2002).
5. E. Aristidi, A. Ziad, J. Chabe, Y. Fantei-Caujolle, C. Renaud, and C. Giordano, "A generalized differential image motion monitor," Mon. Not. R. Astron. Soc. **486**, 915–925 (2019).
6. J. M. Beckers, E. Leon, J. Mason, and L. Wilkins, "Solar Scintillometry: Calibration of Signals and its Use for Seeing Measurements," Sol. Phys. **176**, 23–36 (1997).
7. J. M. Beckers, "A Seeing Monitor for Solar and Other Extended Object Observations," Exp. Astron. **12**, 1–20 (2001).
8. H. Socas-Navarro, J. Beckers, P. Brandt, J. Briggs, T. Brown, W. Brown, M. Collados, C. Denker, S. Fletcher, S. Hegwer, F. Hill, T. Horst, M. Komsa, J. Kuhn, A. Lecinski, H. Lin, S. Oncley, M. Penn, T. Rimmele, and K. Streander, "Solar Site Survey for the Advanced Technology Solar Telescope. I. Analysis of the Seeing Data," Publ. Astron. Soc. Pac. **117**, 1296 (2005).
9. F. Hill, R. Radick, and M. Collados, *Deriving Cn2(h) from a Scintillometer Array*, ATST Site Survey Working Group (ATST, 2003).
10. E. J. Seykora, "Solar Scintillation and the Monitoring of Solar Seeing," Sol. Phys. **145**, 389–397 (1993).
11. J. M. Beckers, "On the relation between scintillation and seeing observations of extended objects," Sol. Phys. **145**, 399–402 (1993).